RESEARCH ARTICLE

Properties of $Li_4Ti_5O_{12}$ as an anode material in non-flammable electrolytes

Beata Kurc · Agnieszka Swiderska-Mocek

Abstract Two non-flammable electrolytes 1 M $LiPF_6$ in sulfolane (TMS) + 5 wt% VC and 0.7 M lithium bis(trifluoromethanesulphonyl)imide ($LiNTf_2$) in *N*-methyl-*N*-propylpyrrolidinium bis(trifluoromethanesulphonyl)imide ($MePrPyrNTf_2$) + 10 wt% gamma-butyrolactone (GBL) were tested with $Li_4Ti_5O_{12}$ (LTO) as highly promising anode material for application in lithium-ion batteries. The results were compared for the titanium anode in the classic electrolyte: 1 M $LiPF_6$ in propylene carbonate + dimethyl carbonate (PC + DMC, 1:1). The performances of LTO/electrolyte/Li cell were tested using cyclic voltammetry, electrochemical impedance spectroscopy, and galvanostatic charge/discharge and scanning electron microscopy (SEM). SEM images of electrodes and those taken after electrochemical cycling showed changes which may be interpreted as a result of solid-state interface formation. Good charge/discharge capacities and low capacity loss at medium C rates preliminary cycling was obtained for the $Li_4Ti_5O_{12}$ anode. For LTO/1 M $LiPF_6$ in PC + DMC/Li system, the best capacity was obtained at C/10 and C/3 (145 and 154 mAh g^{-1}, respectively). In the case of a system working on the basis of a TMS solution (1 M $LiPF_6$ in TMS + 5 wt% VC) the best value was obtained at a C/5 current and an average of more than 150 mAh g^{-1} (86 % of theoretical capacity). For the 0.7 M $LiNTf_2$ in MePrPyrNTf$_2$ + 10 wt% GBL electrolyte, the highest capacitance value (at C/20 current) of about 150 mAh g^{-1} was observed. The 1 M $LiPF_6$ in TMS + 5 wt% VC and 0.7 M $LiNTf_2$ in MePrPyrNTf$_2$ + 10 wt% GBL electrolytes had

a relatively broad thermal stability range and no decomposition peak was observed below 150 °C.

1 Introduction

Lithium-ion batteries are important energy storage devices for portable electronics, power tools, and electrical vehicles [1, 2]. In the past few decades, lithium-ion batteries (LIBs) have been power sources of choice for popular mobile electronic devices such as cellular phones, notebooks and MP3 players [3, 4]. However, a profitable use of LIBs is still limited in the case of large scaled energy storage applications requiring fast charge–discharging power rates [4], e.g., hybrid and electric vehicles (HEVs), renewable energy (wind and solar) plants. Accordingly, it is advisable to explore new nanostructured electrode materials capable of improving the rate performance of LIBs by assuring enhanced kinetics of the solid-state diffusion of the Li^+ intercalation process as well as a high value of electronic conductivity [5]. A promising safe anode alternative to the commercial carbon/graphite is the spinel-type $Li_4Ti_5O_{12}$ (LTO). This material has attracted attention because of the low cost, satisfactory safety and easy preparation. Spinel $Li_4Ti_5O_{12}$ material has an excellent reversibility of Li-ion intercalation and deintercalation with a theoretical capacity of 175 mAh g^{-1} and it also exhibits no volume changes during charge and discharge cycles combined with an excellent safety performance [6–8]. It also has a very flat voltage plateau at around 1.55 V (vs. Li/Li$^+$), which is higher than the reduction potential of most organic

B. Kurc · A. Swiderska-Mocek (✉)
Faculty of Chemical Technology, Poznan University
of Technology, 60 965 Poznan, Poland
e-mail: agnieszka.swiderska-mocek@put.poznan.pl

electrolytes [9–11]. However, the power performance of $Li_4Ti_5O_{12}$ is greatly limited by its low electronic conductivity (ca. 10^{-13} S cm^{-1}) and moderate Li diffusion coefficient (10^{-8}–10^{-11} cm^2 s^{-1}) [12, 13]. In order to improve the electrochemical performance of the $Li_4Ti_5O_{12}$ anode, extensive works concentrated on forming nanoparticles [14–17], doping [18–23] with metal cations and composing with carbon or metal powders [21, 24–29]. The formation of nanoparticles can reduce the Li-ion diffusion path as well as provide a large contact area between the nanoparticles. Doping by other metal cations and adding carbon or metal powder into the $Li_4Ti_5O_{12}$ can increase electronic conductivity. Conventional organic solvents [ethylene carbonate, propylene carbonate (PC), dimethyl carbonate, etc.] used in Li-ion cells are flammable due to their relatively high vapour pressure. Instead of a salt solution in volatile solvents, non-volatile molten salts may be applied as electrolytes. Salts liquid at room temperature, usually called ionic liquids (ILs), are non-volatile solvents and show high thermal, chemical and electrochemical stability. They exhibit a very low vapour pressure and high non-flammability properties that are of importance in their use as safe electrolytes in Li-ion batteries [30–32]. Another approach is to test low vapour pressure molecular solvents, e.g., tetramethylene sulfone (sulfolane, TMS, T_b = 280 °C) [33] or gamma-butyrolactone (GBL, T_b = 205 °C) [34].

The general aim of the present paper was to study the $Li_4Ti_5O_{12}$ anode in two non-flammable electrolytes (1 M $LiPF_6$ in TMS + 5 wt% VC and 0.7 M $LiNTf_2$ in MePrPyrNTf$_2$ + 10 wt% GBL) and compare the results with those for the system $Li_4Ti_5O_{12}$/Li with a classical electrolyte: $LiPF_6$ in PC + DMC (1:1).

2 Experimental

2.1 Materials

Lithium titanate $Li_4Ti_5O_{12}$ powder (Aldrich, BET surface area 32.6 m^2 g^{-1}, mean diameter 940 nm), carbon black (CB, Fluka), poly(vinylidene fluoride) (PVdF, Fluka), sulfolane (TMS, Fluka), gamma-butyrolactone (GBL, Aldrich), vinylene carbonate (VC, Aldrich), lithium foil (Aldrich, 0.75 mm thick), N-methyl-2-pyrrolidinone (NMP, Fluka), propylene carbonate (PC, Aldrich), dimethyl carbonate (DMC, Aldrich), lithium hexafluorophosphate (LiPF$_6$, Fluka) and lithium bis(trifluoromethanesulphonyl)imide (LiNTf$_2$, Fluka) were used as-purchased. N-methyl-N-propylpyrrolidinium bis(trifluoromethanesulphonyl)imide (MePrPyr NTf$_2$) was prepared according to the literature [35] by reacting N-methylpyrrolidinium (Aldrich) with bromopropane (Aldrich) followed by metathesis with LiNTf$_2$. Solid LiNTf$_2$ and LiPF$_6$ salts were dissolved in the liquid salt MePrPyrNTf$_2$

(0.7 M LiNTf$_2$ in MePrPyrNTf$_2$) and liquid TMS heated to ca. 35 °C (1 M LiPF$_6$ in TMS), respectively. Electrolytes containing GBL (0.7 M LiNTf$_2$ in MePrPyrNTf$_2$ + 10 wt% GBL) and VC (1 M LiPF$_6$ in TMS + 5 wt% VC) and a classical electrolyte (1 M LiPF$_6$ in PC + DMC, 1:1) were prepared in a dry argon atmosphere in a glove box. Tested anodes were prepared on a copper foil (Hohsen, Japan) by a casting technique, from a slurry of $Li_4Ti_5O_{12}$, CB and PVdF in NMP. The ratio of components was $Li_4Ti_5O_{12}$:CB:PVdF = 85:5:10 (by weight). After solvent (NMP) vacuum evaporation at 120 °C, a layer of the anode was formed, containing the active material ($Li_4Ti_5O_{12}$), an electronic conductor (CB) and the binder (PVdF).

2.2 Procedures and measurements

Particle size of $Li_4Ti_5O_{12}$ was determined with Zetasizer Nano ZS (Malvern Instruments Ltd., UK). Specific surface areas of $Li_4Ti_5O_{12}$ powders were determined by N$_2$ adsorption (BJH method) using an ASAP 2020 instrument (Micromeritics Instrument Co.). The performance of the cells was characterized using galvanostatic charge–discharge tests, cyclic voltammetry (CV) and electrochemical impedance spectroscopy (EIS). Cycling efficiency of $Li_4Ti_5O_{12}$|Li systems was measured in two compartment cells. Electrodes (metallic-lithium foil and $Li_4Ti_5O_{12}$) were separated by the glass microfiber GF/A separator (Whatman, 0.4 mm thick), placed in an adopted Swagelok$^®$ connecting tube. Typically, the mass of electrodes was as follows: Li: ca. 45 mg (0.785 cm^2) and $Li_4Ti_5O_{12}$: 2.5–3.5 mg. Cells were assembled in a glove box in the dry argon atmosphere. Cycling measurements were taken with the use of the ATLAS 0461 MBI multichannel electrochemical system (Atlas-Sollich, Poland) at different current rates (C/20–C/3). CV and ac impedance measurements were performed using the μAutolab FRA2 type III electrochemical system (Ecochemie, the Netherlands). Flash point of electrolytes was measured with an open cup home-made apparatus, based on the Cleveland open cup instrument, with a 1.5 ml cup. The cup was heated electrically through a sand bath and temperature was measured with the M-3850 digital thermometer (Metex, Korea). The apparatus was scaled with a number of compounds of known flash points. The thermal behaviour of electrolytes in the temperature range of 20–300 °C was studied by DSC. A differential scanning calorimeter model DSC XP-10 (Thass GmbH) was used. After electrochemical measurements, cells were disassembled in a glove box, the electrodes were washed with DMC and dried in vacuum at room temperature. The morphology of the $Li_4Ti_5O_{12}$ electrode (pristine and after electrochemical cycling) was observed under a scanning electron microscope (SEM, Tescan Vega 5153).
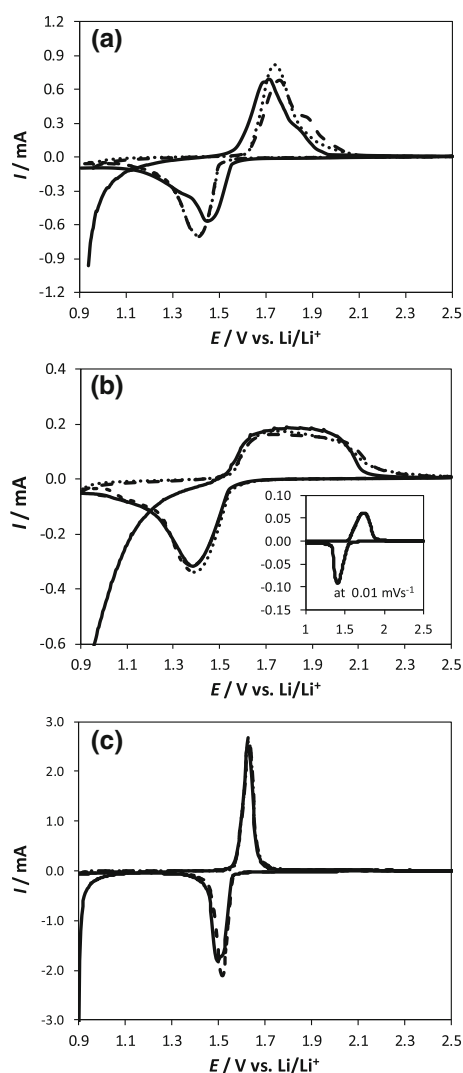
Fig. 1 Cyclic voltammograms of the spinel $Li_4Ti_5O_{12}$ in (a) 1 M LiPF$_6$ in TMS + 5 wt% VC, (b) 0.7 M LiNTf$_2$ in MePrPyrNTf$_2$ + 10 wt% GBL and (c) 1 M LiPF$_6$ in PC + DMC (1:1). Scan rate 0.1 mV s^{-1}. Counter electrode Li

3 Results and discussion

3.1 Cycle voltammetry

Figure 1 presents cyclic voltammograms (CVs) of: $Li_4Ti_5O_{12}$/1 M LiPF$_6$ in TMS + 5 wt% VC/Li, $Li_4Ti_5O_{12}$/ 0.7 M LiNTf$_2$ in MePrPyrNTf$_2$ + 10 wt% GBL/Li and $Li_4Ti_5O_{12}$/1 M LiPF$_6$ in PC + DMC (1:1)/Li cells obtained in the potential window of 1.0–2.5 V at a scan rate of 0.1 mV s^{-1}. Each curve clearly demonstrates that there is one pair of redox peaks in the range of 1.0–2.5 V, which is in accordance with the typical CV characteristics of spinel $Li_4Ti_5O_{12}$ [36]. Oxidation peaks at about 1.65 V and the reduction peak at 1.5 V may be attributed to the oxidation/reduction reactions of the Ti^{3+}/Ti^{4+} couple in the spinel structure, compensated by lithium extraction–

insertion (Fig. 1c). However, compared with $Li_4Ti_5O_{12}$ in classical LiPF$_6$ solutions in cyclic carbonates, the peak currents and separation of the peak area of $Li_4Ti_5O_{12}$ in sulfolane and IL electrolytes are lower and much larger, respectively (Fig. 1a, b). The difference in currents between anodic and cathodic peaks can be mainly attributed to an increase in viscosity of electrolytes (TMS and IL) [37]. In turn, the slow lithium ion diffusivity in the solid-state body of bulk spinel $Li_4Ti_5O_{12}$ may be caused by low lithium salt dissociation and stronger lithium salvation.

3.2 Galvanostatic charging/discharging

Figure 2 shows charge/discharge curves for 2, 10 and 50 cycles for 1 M LiPF$_6$ in TMS + 5 wt% VC, 0.7 M LiNTf$_2$ in MePrPyrNTf$_2$ + 10 wt% GBL and 1 M LiPF$_6$ in PC + DMC (1:1) electrolytes. When sulfolane was used as an electrolyte solvent (Fig. 2a), a capacity of 128 mAh g^{-1} was obtained during the second cycle. This value decreased slightly after subsequent cycles, then finally reached a stable
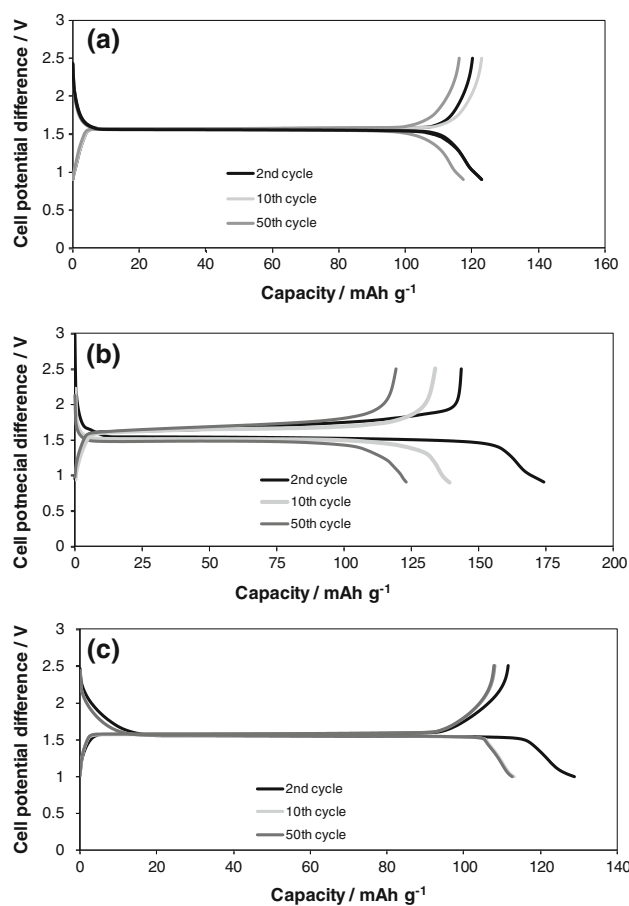

Fig. 2 Galvanostatic charging and discharging of (a) $Li_4Ti_5O_{12}$/1 M LiPF$_6$ in TMS + 5 wt% VC/Li, (b) $Li_4Ti_5O_{12}$/0.7 M LiNTf$_2$ in MePrPyrNTf$_2$ + 10 wt% GBL/Li and (c) $Li_4Ti_5O_{12}$/1 M LiPF$_6$ in PC + DMC (1:1)/Li system (second, tenth, fiftieth cycles) at C/20 rate
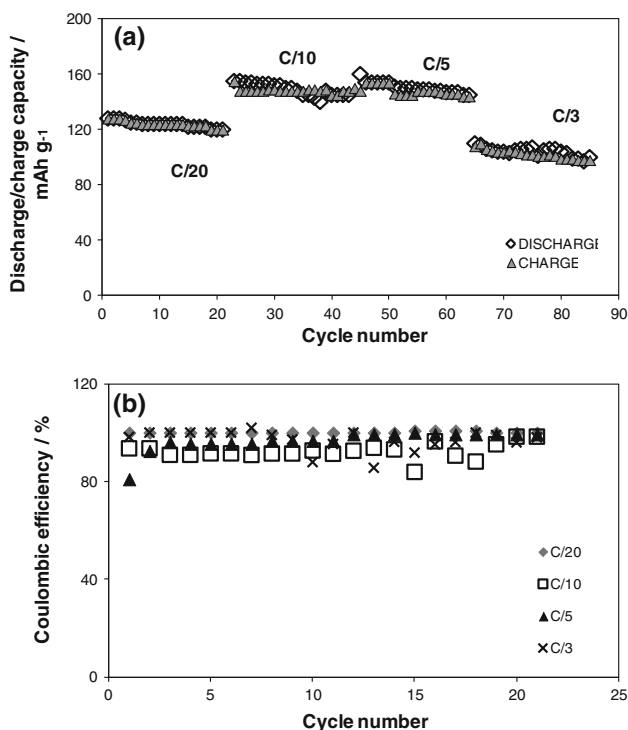
Fig. 3 Charging/discharging capacity (**a**) and Coulombic efficiency (**b**) of the $Li_4Ti_5O_{12}$/1 M LiPF$_6$ in TMS + 5 wt% VC/Li cell
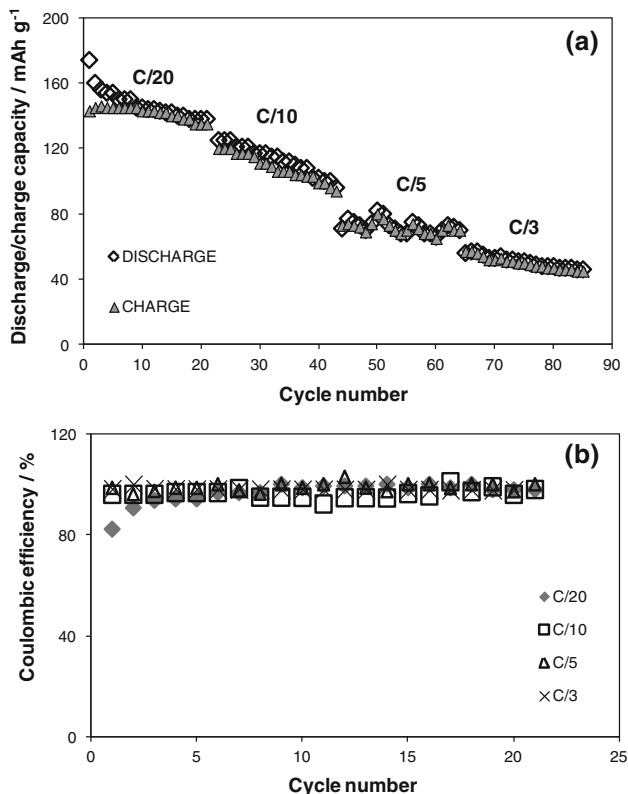

Fig. 4 Charging/discharging capacity (**a**) and Coulombic efficiency (**b**) of the $Li_4Ti_5O_{12}$/0.7 M LiNTf$_2$ in MePrPyrNTf$_2$ + 10 wt% GBL/Li cell

capacity of 120 mAh g^{-1}. This indicates that the capacity after 50 cycles of charge/discharge decreases by about 9 %. A similar situation was found in the case of MePrPyrNTf$_2$ (Fig. 2b). The highest capacity for both intercalation and deintercalation was found in the second cycle of the process (174 and 143 mAh g^{-1}, respectively). A 100 % reversibility of the cells was reached after only ten cycles. During at the first three cycles formed of so-called SEI layer. Its formation is always associated with a loss of capacity.

In subsequent cycles of the charge and discharge processes, the capacity decreased slightly to reach (after 50 cycles) the value of 120 and 123 mAh g^{-1}, respectively. The fastest stabilization of the capacity was observed (Fig. 2c) in the case of the classical electrolyte (1 M LiPF$_6$ in PC + DMC). It occurred after ten charge/discharge cycles, maintaining the same value for both the processes (ca. 110 mAh g^{-1}, which is 63 % of the theoretical capacity). Charging/discharging curves for the $Li_4Ti_5O_{12}$/1 M LiPF$_6$ in TMS + 5 wt% VC/Li cell are shown in Fig. 3a. The charging and discharging capacity of the $Li_4Ti_5O_{12}$ anode was between 160 and 80 mAh g^{-1} for different rates (C/2, C/5, C/10 and C/20). In the case of a system working on the basis of a TMS solution, the best value was obtained at a C/5 rate and an average of more than 150 mAh g^{-1} (86 % of theoretical capacity). The highest capacitance was observed for the $Li_4Ti_5O_{12}$/0.7 M LiNTf$_2$ in MePrPyrNTf$_2$ + 10 wt% GBL/Li (Fig. 4a) at a C/20 rate
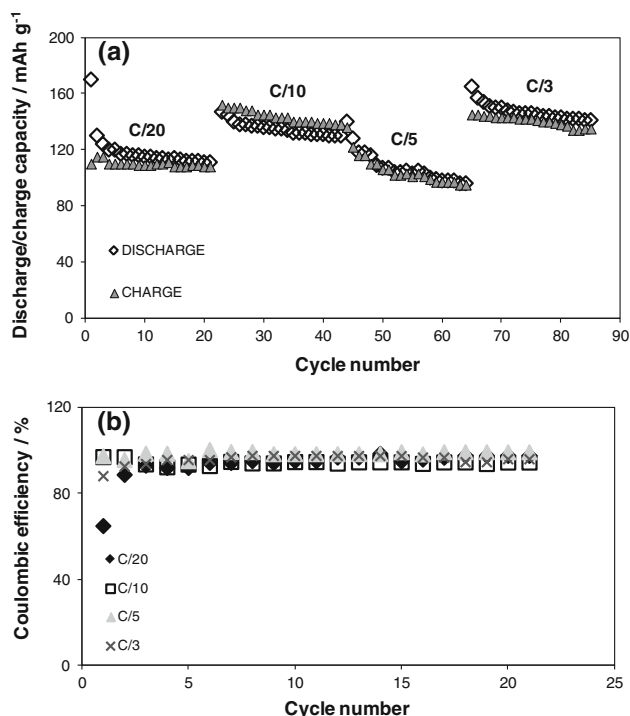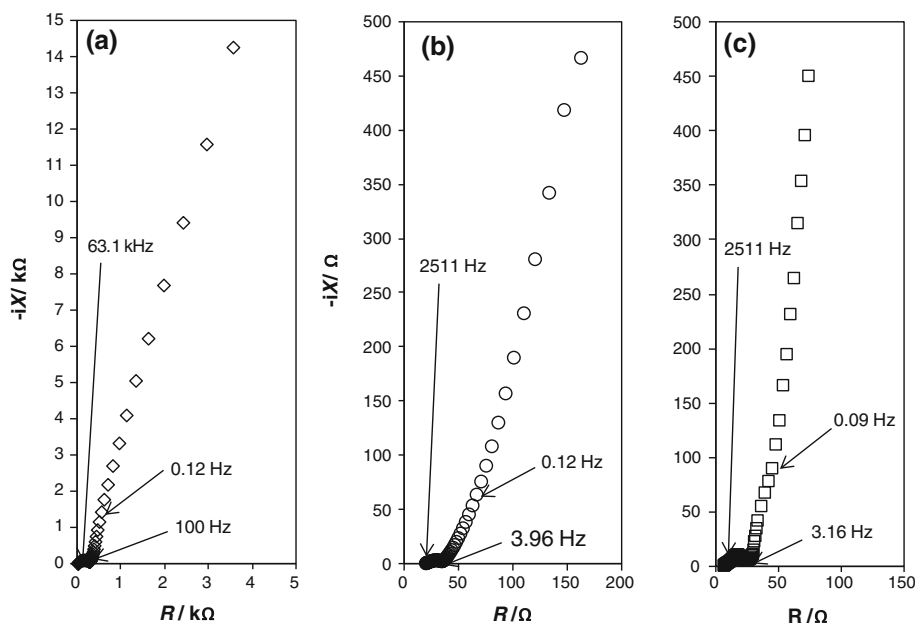

Fig. 5 Charging/discharging capacity (**a**) and Coulombic efficiency (**b**) of the $Li_4Ti_5O_{12}$/1 M LiPF$_6$ in PC + DMC (1:1)/Li cell

Fig. 6 Impedance spectroscopy of (**a**) $Li_4Ti_5O_{12}$/0.7 M $LiNTf_2$ in $MePrPyrNTf_2$ + 10 wt% GBL/Li, (**b**) $Li_4Ti_5O_{12}$/1 M $LiPF_6$ in TMS + 5 wt% VC/Li and (**c**) $Li_4Ti_5O_{12}$/1 M $LiPF_6$ in PC + DMC (1:1)/Li systems recorded after cell assembling (OCV $\sim$3.1 V). Frequency range 10^5–10^{-2} Hz

(approx. 150 mAh g^{-1}). When the current regime was increased to C/3, that value decreases to 60 mAh g^{-1}. In contrast, for $Li_4Ti_5O_{12}$/1 M $LiPF_6$ in PC + DMC (Fig. 5a) the best capacities were obtained at C/10 and C/3, amounting to 145 and 154 mAh g^{-1}, respectively. The efficiency of the process of insertion and deinsertion was 98 %.

That is to say, the structure of $Li_4Ti_5O_{12}$ is not destroyed during the charge/discharge cycling. Probably the loss of capacity fluctuation on the capacity-cycle profile at this high current rate also suggests that Li$^+$ insertion/extraction only takes place in the $Li_4Ti_5O_{12}$ grains at near the outer surface of the highly aggregated particles. The capacity is much low at high current rates, and needs to be improved.

Coulombic efficiency of the process was found to be close to 95–99 % ($\pm$4 %), depending on the discharge rate and it was identical for all the three electrolytes (Figs. 3b, 4b, 5b). However, it can be seen that in the case of the lowest C/10 rate it was 90 % for the TMS-based electrolyte (Fig. 1a).

3.3 Impedance spectroscopy (SEI formation)

Anodes characterized by a low potential, such as lithium metal or lithiated graphite, react spontaneously with electrolytes. In the case of lithium metal, the growth of dendrite crystals on its surface is observed. It has also been shown that lithiated graphite requires the formation of a protective coating, similarly to metallic lithium. Consequently, the electrolyte for Li-ion batteries is expected to form SEI, protecting the lithium anode [38]. A similar phenomenon has also been found for the $Li_4Ti_5O_{12}$ anode. A solid electrolyte interface can be formed on the $Li_4Ti_5O_{12}$ anode after several cycles. This is different in the case of a

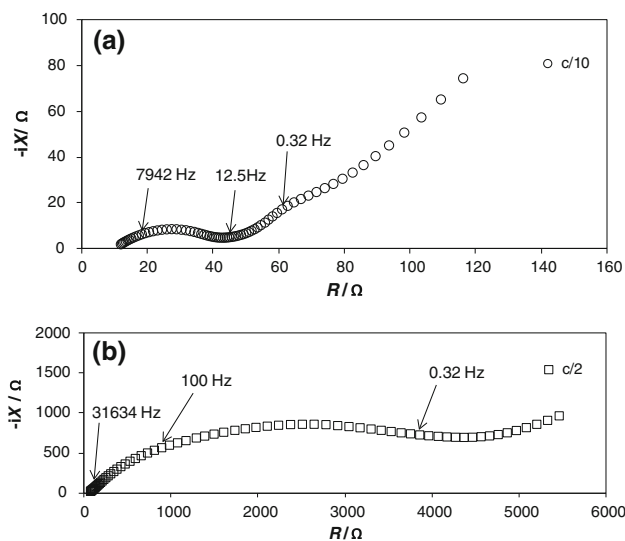**Fig. 7** Impedance spectroscopy of the $Li_4Ti_5O_{12}$/1 M $LiPF_6$ in TMS + 5 wt% VC/Li cell after 20 cycles of galvanostatic charging/discharging at various rates: (**a**) C/10 (OCV 1.59 V) and (**b**) C/2 (OCV 1.56 V). Frequency range 10^5–10^{-2} Hz

Fig. 8 Impedance spectroscopy of the $Li_4Ti_5O_{12}$/0.7 M $LiNTf_2$ in $MePrPyrNTf_2$ + 10 wt% GBL/Li cell after 20 cycles of galvanostatic charging/discharging at various rates: C/10 (OCV 1.51 V) and C/2 (OCV 1.59 V). Frequency range 10^5–10^{-2} Hz
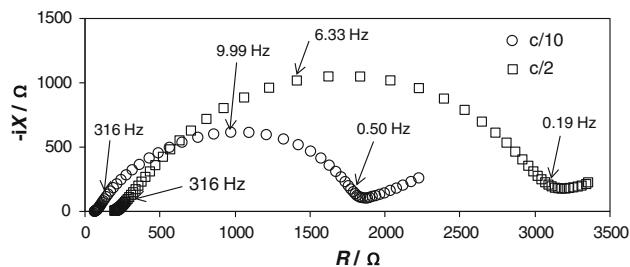
graphite anode where the SEI film forms during the initial cycle [39, 40]. The passivation of electrodes in a Li-ion battery may be observed with the help of impedance spectroscopy. Electrochemical impedance spectra (EIS) of the LTO/electrolyte/Li were measured before discharge and after 20 cycles (at C/10 and C/2 rates). The impedance spectra were recorded in two electrode cells using Li counter. Then, the EIS results also include impedance of
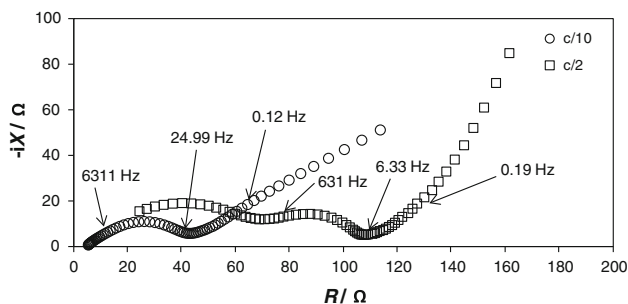

Fig. 9 Impedance spectroscopy of the $Li_4Ti_5O_{12}$/1 M $LiPF_6$ in PC + DMC (1:1)/Li cell after 20 cycles of galvanostatic charging/discharging at various rates: C/10 (OCV 1.56 V) and C/2 (OCV 1.63 V). Frequency range 10^5–10^{-2} Hz
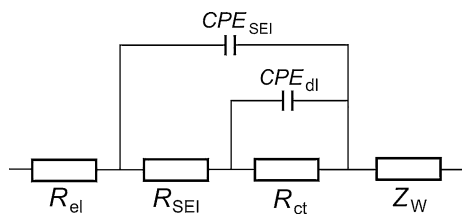

Fig. 10 An equivalent circuit representing the electrode/electrolyte system

lithium interface. Figure 6 shows impedance of three: $Li_4Ti_5O_{12}$/0.7 M $LiNTf_2$ in $MePrPyrNTf_2$ + 10 wt% GBL/Li, $Li_4Ti_5O_{12}$/1 M $LiPF_6$ in TMS + 5 wt% VC/Li and $Li_4Ti_5O_{12}$/1 M $LiPF_6$ in PC + DMC/Li unsymmetrical cells before cycling. As it can be seen, spectra taken immediately after the cell assembling consisted of a semicircle, followed by a long linear part. The semicircle can be attributed to phenomena such as polarization resistance and the formation of the SEI layer. The distinct linear part is due to the diffusion of Li^+ in the electrolyte and SEI, or Li in a solid electrode (insertion/extraction). It may be noted that the high lithium diffusion resistance in the anode material may be the rate-determining step. The diffusion coefficient D of the lithium ions diffusing in the $Li_4Ti_5O_{12}$ is ca. 1×10^{-10}–1×10^{-11} cm^2 s^{-1} [13]. However, after galvanostatic charging/discharging cycles at different rates (Figs. 7, 8, 9) a flat quasi-semicircle or two semicircles can be seen at the high-frequency region and a short straight line at the low-frequency region. The first semicircle reflects the formation of the SEI layer and the second the charge transfer process, while the line at the low-frequency region represents the diffusion process. The equivalent circuit used for impedance spectra deconvolution (Fig. 10) consists of two RC elements describing resistance of SEI (R_{SEI}) and resistance of the charge transfer reaction (R_{ct}), in series with electrolyte resistance R_{el} and diffusion impedance represented by the Warburg element (Z_W). It can be seen that impedance for all the three increases with the current rate increase. Charge transfer resistances (R_{ct}) (Fig. 8) were found to be 1,550 and 2,890 Ω for $Li_4Ti_5O_{12}$/0.7 M $LiNTf_2$ in MePrPyrNTf_2 + 10 wt% GBL/Li cell at C/10 and C/2 rates, respectively, indicating a high kinetic barrier. However, a much smaller increase of impedance was observed in the case of the 1 M $LiPF_6$ in TMS + 5 % VC (just 120 Ω
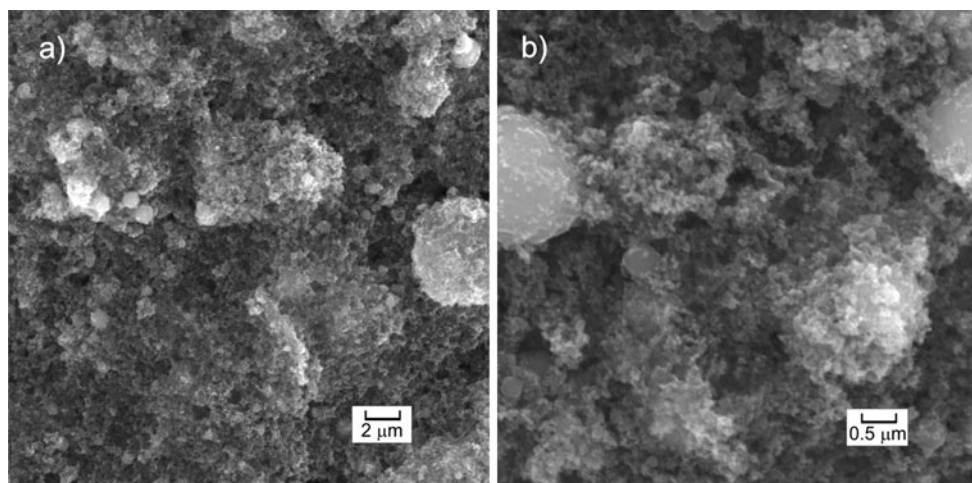

Fig. 11 SEM images of the pristine $Li_4Ti_5O_{12}$ anode. Magnification $\times 5,000$ (a) and $\times 20,000$ (b)

at C/10 rate) system (Fig. 7). Then, the SEI resistance and the charge transfer resistance were 31 and 14 Ω at a C/10 rate, respectively. In the case of the 1 M $LiPF_6$ in PC + DMC (1:1) electrolyte impedance spectrum had a shape of a semicircle followed by a line (Fig. 9) when the system was charged/discharged at a low rate (C/10). However, after charging/discharging at higher rates (C/2 rate) two semicircles were present in the spectrum. The charge transfer resistance and the SEI resistance were 104

and 12 Ω at a C/2 rate, respectively. The particle morphologies of pristine $Li_4Ti_5O_{12}$ and $Li_4Ti_5O_{12}$ after 50 cycles of galvanostatic charging/discharging at different electrolytes observed by SEM are shown in Figs. 11 and 12, respectively. The pristine LTO powders (Fig. 11) had a spherical shape, dense structure and non-aggregation characteristics. The size of the LTO particles was in the micron range (0.5–2 µm). As shown in Fig. 12c, d, the spherical morphology and microstructures slightly changed

Fig. 12 SEM images of the $Li_4Ti_5O_{12}$ anode after 20 charge/discharge cycles at C/10 rate. Electrolyte: 1 M $LiPF_6$ in TMS + 5 wt% VC (**a, b**), 0.7 M $LiNTf_2$ in MePrPyrNTf$_2$ + 10 wt% GBL (**c, d**) and 1 M $LiPF_6$ in PC + DMC (1:1) (**e, f**). Magnification: ×5,000 (**a, c, e**) and ×20000 (**b, d, f**)
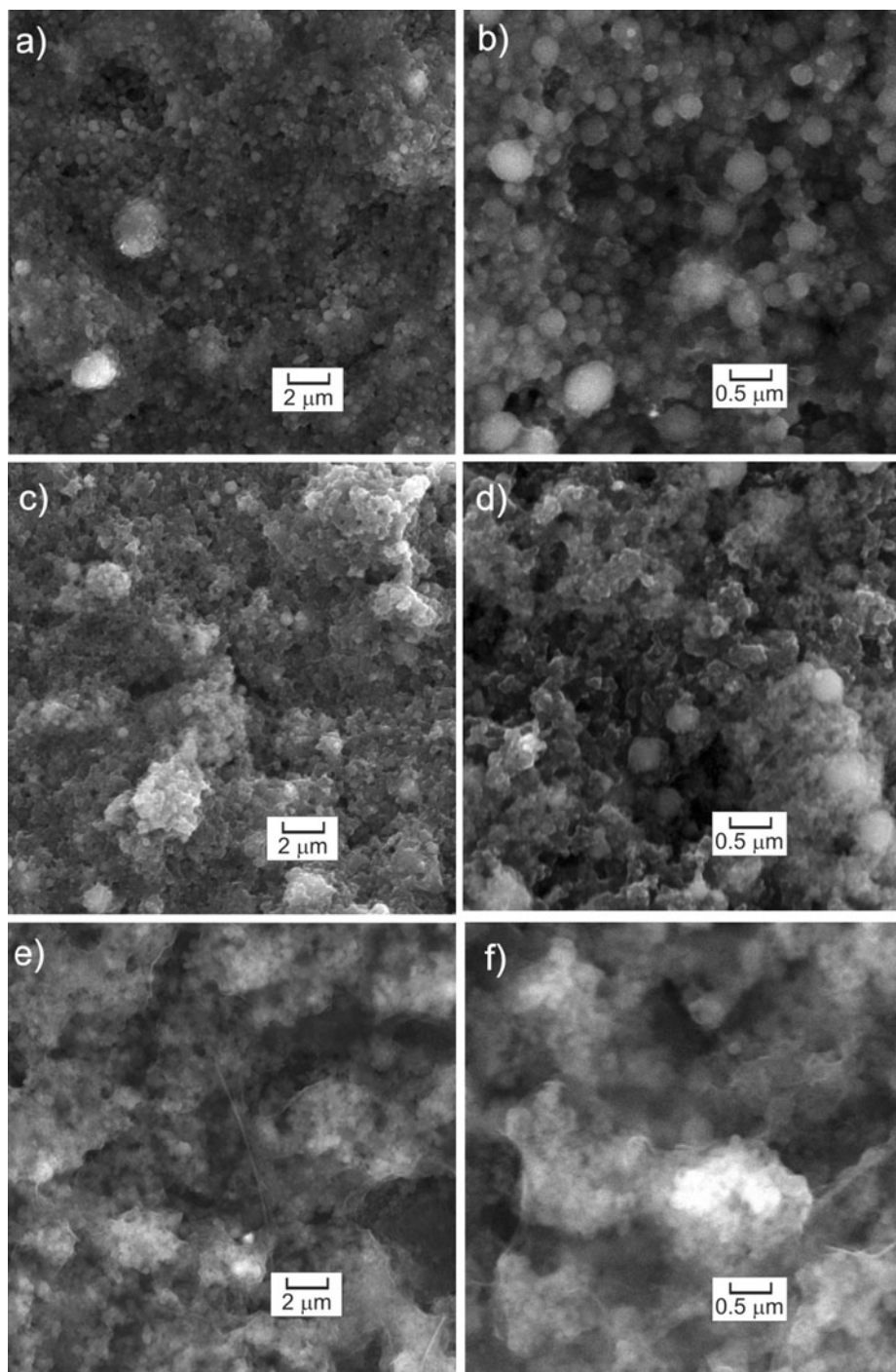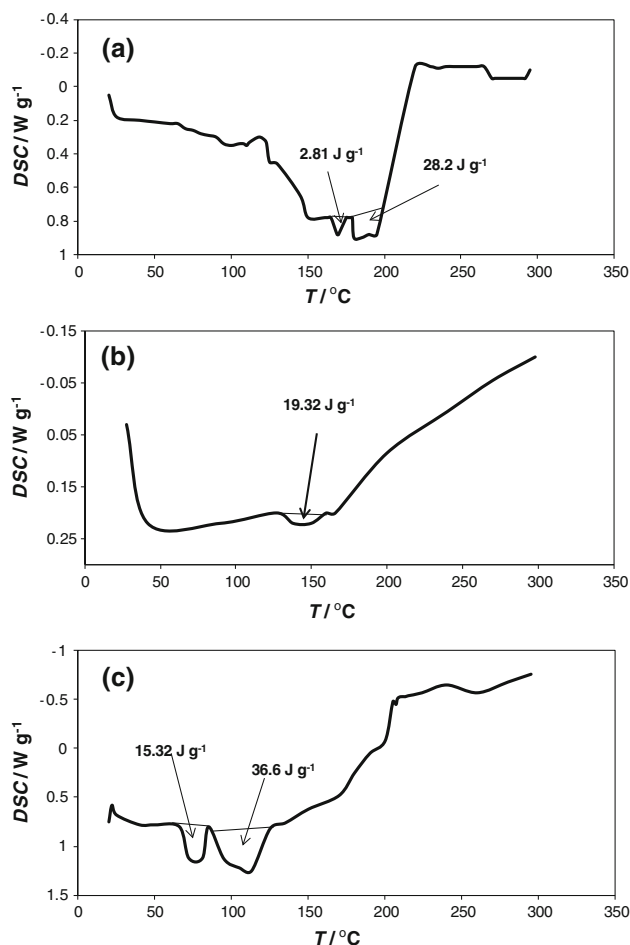
Fig. 13 DSC profiles related to the heating test of the (**a**) $Li_4Ti_5O_{12}$ + 1 M $LiPF_6$ + TMS + 5 wt% VC, (**b**) $Li_4Ti_5O_{12}$ + 0.7 M $LiNTf_2$ in MePrPyrNTf$_2$ + 10 wt% GBL, (**c**) $Li_4Ti_5O_{12}$ + 1 M $LiPF_6$ in PC + DMC (1:1) electrolyte (nitrogen atmosphere)

after galvanostatic charging/discharging at 0.7 M $LiNTf_2$ in MePrPyrNTf$_2$ + 10 wt% GBL (changes are visible only at higher magnifications). However, SEM images of the LTO particles after galvanostatic charging/discharging at 1 M $LiPF_6$ in TMS + 5 % VC and 1 M $LiPF_6$ in PC + DMC (1:1) in Fig. 12a, b, e, f show that they were coated by a uniform layer. Probably this film can be identified as the SEI layer.

3.4 Electrolyte ignition point

The flash point of ethylene carbonate and propylene carbonate is 143 and 132 °C, respectively, while in the case of DMC it is only 16 °C (data from a Sigma-Aldrich catalogue). The flash point of neat sulfolane is much higher 177 °C [41] and the MePrPyrNTf$_2$ is a non-volatile solvent. Only SEI-forming additives (VC, GBL) may increase volatility of the investigated electrolytes. Flash points of the VC and the GBL are 73 and 98 °C, respectively (Sigma-Aldrich catalogue).

On the other hand, during SEI formation the volatile additive is converted into a solid polymeric component of the interface. Probably, also GBL molecules in 0.7 M $LiNTf_2$ in MePrPyrNTf$_2$ are involved in ion salvation. Consequently, the amount of the volatile compound decreases to a low value, increasing the flash point of the electrolyte. The flash point determined for the $LiNTf_2$ solution in MePrPyrNTf$_2$, with GBL is 152 °C. In turn, the system under study, i.e., 1 M $LiPF_6$ + TMS + 5 wt% VC, shows a flash point of ca. 160 °C. Figure 13 presents thermal gravimetric analysis (DSC) of the (a) $Li_4Ti_5O_{12}$ + 1 M $LiPF_6$ + TMS + 5 wt% VC; (b) $Li_4Ti_5O_{12}$ + 0.7 M $LiNTf_2$ in MePrPyrNTf$_2$ + 10 wt% GBL; (c) $Li_4Ti_5O_{12}$ + 1 M $LiPF_6$ in PC + DMC (1:1) electrolyte under nitrogen atmosphere. In the case of the electrolyte based on sulfolane (Fig. 13a), two peaks can be observed at 160 °C (2.81 J g^{-1}) and 180 °C (28.1 J g^{-1}), corresponding to the boiling point of VC (162 °C) and flash point of TMS (177 °C), respectively. Energy transformation in the vicinity of 140–150 °C amounting to 19.32 J g^{-1} can probably answer GBL ignition of the temperature flash point when added to 0.7 M $LiNTf_2$ in MePrPyrNTf$_2$ liquid (Fig. 13b). In the case of the classical electrolyte, again two peaks can be seen (15.32 and 36.6 J g^{-1}) at a temperature of 70–80 and 90–110 °C, which is probably associated with boiling temperatures of solvents used (PC and DMC, Fig. 13c) [41].

4 Conclusions

LTO have a working potential at 1.55 V against lithium which is above the voltage where electrochemical decomposition of the electrolyte takes place for most of the common electrolytes. This work is connected with testing the performance of work, a $Li_4Ti_5O_{12}$ anode using a non-flammable electrolyte with a low vapour pressure, such as 1 M $LiPF_6$ + TMS + 5 wt% VC and 0.7 M $LiNTf_2$ in MePrPyrNTf$_2$ + 10 wt% GBL. The $Li_4Ti_5O_{12}$/Li batteries were investigated by EIS and SEM techniques.

1. SEM images of LTO particles after galvanostatic charging/discharging show that they were covered with relatively uniform layers with conglomerates, which can be identified as a protective SEI coating.
2. Capacity of the LTO anode depends on the current rate (C/20, C/10, C/5 or C/3) and the electrolyte. In the case of a system working on the basis of a TMS solution the best value was obtained at a C/5 current and an average of more than 150 mAh g^{-1} (86 % of theoretical capacity). For $Li_4Ti_5O_{12}$/0.7 M $LiNTf_2$ in MePrPyrNTf$_2$ + 10 wt% GBL/Li the largest capacitance value may be observed at a C/20 current (it is about 150 mAh g^{-1}) and it decreases at higher currents.

However, for $Li_4Ti_5O_{12}$/1 M $LiPF_6$ in PC + DMC (1:1) the best capacity was obtained at C/10 and C/3, amounting to 145 and 154 mAh g^{-1} (which represents about 85 % of the theoretical capacity). Coulombic efficiency of the discharging process was found to be close to 95–99 % ($\pm$4 %), depending on the discharge rate and was the same for all three electrolytes. All the results obtained indicate that LTO anode may be successfully used in lithium-ion batteries.

3. The 1 M $LiPF_6$ in TMS + 5 wt% VC and 0.7 M $LiNTf_2$ in $MePrPyrNTf_2$ + 10 wt% GBL electrolytes had a greater thermal stability and no DSC peak was observed below 150 °C. The classical electrolyte (1 M $LiPF_6$ in PC + DMC) was stable only to a temperature of about 75 °C.

These results suggest that IL ($MePrPyrNTf_2$) and sulfolane (TMS) electrolytes were a good candidate to be safely used as an electrolyte in LIBs.

References

1. Winter M, Besenhard JO, Spahr ME, Novak P (1998) Adv Mater 10:725–763
2. Park KS, Benayad A, Kang DJ, Doo SG (2008) J Am Chem Soc 130:14930–14931
3. Armand M, Tarascon JM (2008) Nature 451:652–657
4. Bruce PG, Scrosati B, Tarascon JM (2008) Angew Chem Int Ed 47:2930–2946
5. Arico AS, Bruce PG, Scrosati B, Tarascon JM, Van Schalkwijk W (2005) Nat Mater 4:366–377
6. Ferg E, Gummow RJ, Kock AD, Thackeray MM (1994) J Electrochem Soc 141:L145–L147
7. Ohzuku T, Ueda A, Yamamoto N (1995) J Electrochem Soc 142:1431–1435
8. Aldon L, Kubiak P, Womes M, Jumas JC, Olivier-Fourcade J, Tirado JL, Corredor JI, Vicente CP (2004) Chem Mater 16:5721–5725
9. Zhang SS, Xu K, Jow TR (2006) Electrochim Acta 51:1636–1640
10. Schranzhofer H, Bugajski J, Santner HJ, Korepp C, Möller KC, Besenhard JO, Winter M, Sitte W (2006) J Power Sources 153:391–395
11. Zhang SS, Xu K, Jow TR (2004) J Power Sources 130:281–285
12. Chen CH, Vaughey JT, Jansen AN, Dees DW, Kahaian AJ, Goacher T, Thackeray MM (2001) J Electrochem Soc 148:A102–A104
13. Doi T, Iriyama Y, Abe T, Ogumi Z (2005) Chem Mater 17:1580–1583
14. Guerfi A, Sevigny S, Lagace M, Hovington P, Kinoshita K, Zaghib K (2003) J Power Sources 119–121:88–94
15. Cheng L, Liu HJ, Zhang JJ, Xiong HM, Xia YY (2006) J Electrochem Soc 153:A1472–A1477
16. Abe Y, Matsui E, Senna M (2007) J Phys Chem Solids 68:681–686
17. Yi TF, Shu J, Zhu YR, Zhu XD, Zhu RS, Zhou AN (2010) J Power Sources 195:285–288
18. Capsoni D, Bini M, Massarotti V, Mustarelli P, Chiodelli G, Azzoni CB, Mozzati MC, Linati L, Ferrari S (2008) Chem Mater 20:4291–4298
19. Wolfenstine J, Allen JL (2008) J Power Sources 180:582–585
20. Huang SH, Wen ZY, Zhu XJ, Gu ZH (2004) Electrochem Commun 6:1093–1097
21. Huang S, Wen Z, Lin B, Han J, Xu X (2008) J Alloys Compd 457:400–403
22. Ji S, Zhang J, Wang W, Huang Y, Feng Z, Zhang Z, Tang Z (2010) Mater Chem Phys 123:510–518
23. Wang J, Liu XM, Yang H, Shen XD (2011) J Alloys Compd 509:712–718
24. Wang GJ, Gao J, Fu LJ, Zhao NH, Wu YP, Takamura T (2007) J Power Sources 174:1109–1112
25. Huang JJ, Jiang ZY (2008) Electrochim Acta 53:7756–7759
26. Li X, Qu MZ, Huai YJ, Yu ZL (2010) Electrochim Acta 55:2978–2982
27. Li X, Qu MZ, Yu ZL (2010) Solid State Ionics 181:635–639
28. Yuan T, Yu X, Cai R, Zhou YK, Shao ZP (2010) J Power Sources 195:4997–5004
29. Webber A, Blomgren GE (2002) In: van Schalkwijk WA, Scrosati B (eds) Advances in lithium-ion batteries. Kluwer, New York
30. Lewandowski A, Swiderska-Mocek A (2009) J Power Sources 194:601–609
31. Guerf A, Dontigny M, Charest P, Petitclerc M, Lagace M, Vijh A, Zaghib K (2010) J Power Sources 195:845–852
32. Lewandowski A, Kurc B, Stepniak I, Swiderska-Mocek A (2011) Electrochim Acta 56:5972–5978
33. Kinoshit SC, Kotato M, Sakata Y, Ue M, Watanabe Y, Morimoto H, Tobishima SI (2008) J Power Sources 183:755–760
34. Lewandowski A, Swiderska-Mocek A (2009) J Power Sources 194:502–507
35. Wang YG, Li HM, Wang KX, EiJi H, Wang YR, Zhou HS (2009) J Mater Chem 19:6789–6795
36. Li J, Tang Z, Zhang Z (2005) Electrochem Commun 7:894–899
37. Aurbach D (2000) J Power Sources 89:206–218
38. Ding Y, Li GR, Xiao CW, Gao XP (2013) Electrochim Acta 102:282–289
39. Shu J (2008) Electrochem Solid State Lett 11:A238–A240
40. Wu F, Wang Z, Li X, Wu L, Wang X, Zhang X, Wang Z, Xiong X, Guo H (2011) J Alloys Compd 509:596–601
41. Martinmaa J (1976) Sulfolane. In: Lagowski JJ (ed) The chemistry of nonaqueous solvents. Academic Press, New York